Mechanism of the Formation of High-Energy Phase-Structure States under Various Conditions of Ion Implantation

A.D. Korotaev, A.N. Tyumentsev*, and S.P. Bugaev**

Siberian Physicotechnical Institute, 1 Novosobornaja Sq., Tomsk 634050, Russia,
(3822) 230394, (3822) 233034, korotaev@phys.tsu,ru
** Institute of Strength Physics and Materials Science, Siberian Division, Russian Academy of Sciences,*
2/1 Akademichesky Av., Tomsk 634055, Russia,
*** Institute of High Current Electronics, Siberian Division, Russian Academy of Sciences,*
4 Akademichesky Av., Tomsk 634055, Russia

Abstract – The electron microscopy method was used to examine the structure-phase states of the ion-implanted layer in molybdenum and austenitic stainless steels in relation to the degree of vacuum, the temperature, and the implanted ion dose and type. It has been demonstrated that the adsorption and mixing of the reactive components of the residual gas in the target material have the result that, whatever the type of implanted ions, nanoparticles of carbides, nitrides or oxides are formed. Suppression of the processes of structural relaxation is the determining factor in the formation of highly nonequilibrium states with a density of uniformly distributed dislocations of up to 10^{11} cm^{-2} and a lattice curvature of 10–30 deg/μm. As the implanted ion dose is increased and the temperature is decreased, amorphous-crystalline and amorphous states occur in the surface layer. The relation of the nature of the phases formed upon ion implantation to the enthalpy of their formation for the target material and for the components of the residual gas of the implanter is discussed.

1. Introduction

The modification of the structure and physical and mechanical characteristics of a solid by ion implantation (II) is associated with ion doping combined with the development of a defect substructure in a narrow surface layer (Δh = 200–300 nm) [1–3]. Therefore, besides the type and dose of the implant ions, their energy, and the beam current density, of critical importance in imparting desired operating characteristics to metals and alloys treated with ion beams is the partial pressure of the gaseous components of the vacuum medium of the implanter. Surface adsorption of the gas medium components, such as N, C, and O, their ionic mixing and radiation-enhanced diffusion can change substantially not only the elemental composition, but also the features of the phase-structure state formed practically throughout the depth of the ion-doped layer. The related inhibition of the dislocation and structural relaxation in this layer due to the formation of anomalously supersaturated interstitial solid solutions, highly dispersed carbides, nitrides, oxides, and more composite compounds offer an opportunity of the formation of high-energy defect substructures [1–3], up to solid-phase amorphization [4–5], which are not observed for the II of the chosen types of ions. Moreover, for the same type of ions, depending on the degree of vacuum and on the ion beam current density, various phase-structure states and, hence, operating characteristics of materials and articles treated by the II method can be obtained. Thus, upon implantation of Ti ions into α-Fe and stainless steel in a vacuum of 10^{-6} Torr, amorphization of the surface layer due to its saturation with carbon was observed which was accompanied by a considerable decrease of the coefficient of friction and an enhancement of the resistance to wear [6, 7]. Amorphization was observed [8] upon self-implantation of chromium due to the saturation of the surface with oxygen from the gas medium of the implanter in vacuum. As shown in [9], the saturation of the surface layer in II is detected even for a vacuum of 10^{-8} Torr.

At the same time, the demands for economic efficiency of the II technology of AI and the necessity of using high doses ($\geq 5\cdot10^{16}$–10^{17} cm^{-2}) to improve the operating characteristics of articles made of metallic materials call for implanters with comparatively poor vacuum (~10^{-5} Torr), high ion current density, and, hence, a heatable target. In this case, as a rule, the influence of the gas medium of the implanter is ignored.

This paper describes an experiment where electron microscopy in thin metal foils was used, **first**, to examine the evolution of the phase-structure state in the surface layer of molybdenum in relation to the dose of carbon, nitrogen, molybdenum, yttrium, titanium, and zirconium implant ions (10^{16}–$5\cdot10^{17}$ cm^{-2}) in a vacuum of $2\cdot10$–$4\cdot10^{-5}$ Torr with high partial pressures of hydrocarbons and oxygen, produced by a diffusion pump. Besides, the composition of the gas medium of the implanter was varied by feeding nitrogen at a partial pressure of $4\cdot10^{-4}$ Torr into the working chamber. This made it possible to compare the features of phase

formation on direct implantation of interstitial atoms into the target lattice and on introduction of these atoms as a result of ion mixing and radiation-enhanced diffusion during implantation of metal ions (Y, Mo, Ti, and Zr). **Second**, a comparative examination of the phase-structure states formed under identical II conditions has been performed for metal targets (molybdenum, stainless steel) showing a different activity to the elements of the implanter gas medium. **Third**, such an examination has been performed for II carried out in a cryogenic vacuum of 10^{-6}–10^{-7} Torr, and the results have been compared with the data obtained in a vacuum of 10^{-4}–10^{-5} Torr produced by a diffusion pump.

2. Experimental Technique and Materials

The principal investigations were carried out on recrystallized samples (20×20×0.1 mm) of undoped molybdenum and type chromium-nickel austenitic stainless steel with grain size d = 30–50 μm and initial dislocation density $\rho_0 = (2–5)\cdot10^8$ cm^{-2}. For comparison, at low ($\leq 5\cdot10^{16}$ cm^{-2}) doses of carbon and titanium ions, samples of recrystallized α-Fe were also used as targets. The metals chosen as implants (Ti, Zr, Y) are substantially different by atomic radius, electronegativity, and equilibrium solubility in the target materials owing to which the intensity of internal stresses formed in nonequilibrium solid solutions on II – a key factor in modification of the defect substructure – was different. With molybdenum targets, Mo and Pb ions were also used, making possible to vary the mass of implant ions over a wide range.

Ion implantation was carried out on Titan, a pulsed ion implanter designed at the Institute of High Current Electronics (Tomsk) [10]. The ion irradiation modes and conditions are presented in Table 1.

The samples for electron-microscopic examinations were prepared by jet electropolishing on the side not subject to irradiation. Used as electrolyte was a mixture of chloric (20%) and acetic (80%) acids for Fe-base alloys and a 20% solution of sulfuric acid in methanol for molybdenum with the potential difference across the electrolytic cell equal to 40 and 50 V, respectively.

3. Results

3.1. Phase-structure states at implant ion doses $\leq (1–2)\cdot10^{16}$ cm^{-2}

For any mode of ion implantation of metal ions at $T < 400$ K, electron micrographs of the surface layer show the so-called "speckled" contrast [11, 12], testifying to the formation of clusters of point defects, shallow dislocation loops, and, perhaps, highly dispersed ($d < 5$ nm) particles. For the implantation of titanium ions into α-Fe and Y, Ti, Si, and Pb ions into Mo, no change in electron diffraction pattern was revealed. This suggests that second phases are not formed in an ion-doped layer. This has been confirmed by the results of microstructure analyses performed after annealing of ion-doped Mo at T = 1200 K which results in the coagulation of dislocation loops and in the annihilation of vacancies that persist in the lattice upon irradiation which is accompanied by an increase in loop size by an order of magnitude and more [12].

The results of examination of the phase-structure state of an ion-doped layer after implantation of carbon and nitrogen ions are substantially different. Though "speckled" contrast [11, 12] is also detected in this case, the presence of highly dispersed carbides or nitrides is evidenced by the diffuse electron diffraction peaks between and near the main reflexes (Fig. 1,*a*). Second phase particles of size $d \leq 3–4$ nm is directly observed in dark-field micrographs (Fig. 1,*b*). The distribution profiles of carbon and nitrogen in Mo calculated by the Monte-Carlo method have shown [13] that their maximum concentration at a radiation dose of 10^{16} cm^{-2} reaches $C_{max} \approx 0.8$ at. %, which considerably exceeds the solubility of these interstitial elements in Mo at $T \leq 400$ K [14].

Table 1. Modes of ion implantation

Mode	Medium	Ion type	Target material	Ion energy, keV	Pulse frequency, Hz	Current density, mA/cm^2	T, K at the end of II
I.1	Vacuum*	Y, Mo, Pb, Ti, Si	Mo	80	50	1.0	360–370
I.2	– « –	C, N	Mo	80	50	1.0	360–370
II.1	Ar**	Y, Mo, Zr	Mo	80	50	2.0	660
III.1	N**	Y, Mo, Si, Zr	Mo	80	50	1.0	360–370
III.2	– « –	Zr	Mo	30	50	2.0	480
III.3	– « –	Zr	Mo	60	50	2.0	800
IV	Vacuum*	Ti	α-Fe	80	50	1.0	400
V	– « –	Y, Ti, Ni, Cr	Steel	60	50	1.0	400
VI.1	Vacuum*** 10^{-5} Torr	Y, Ti, Ni, Cr	Mo	50	5	7	320
VI.2	Vacuum*** $4\cdot10^{-7}$ Torr	Y, Ti, Ni, Cr	Mo	50	50		320
VI.3	Vacuum*** $2\cdot10^{-6}$ Topp	Y, Ti, Ni, Cr	Steel	50	50		320

* Diffusion pumping, $P \cong (1–2)\cdot10^{-4}$ Torr; ** diffusion pumping with bleed-in of argon or nitrogen, $P \cong (2–4)\cdot10^{-4}$ Torr; *** vacuum produced by cryogenic pumps.

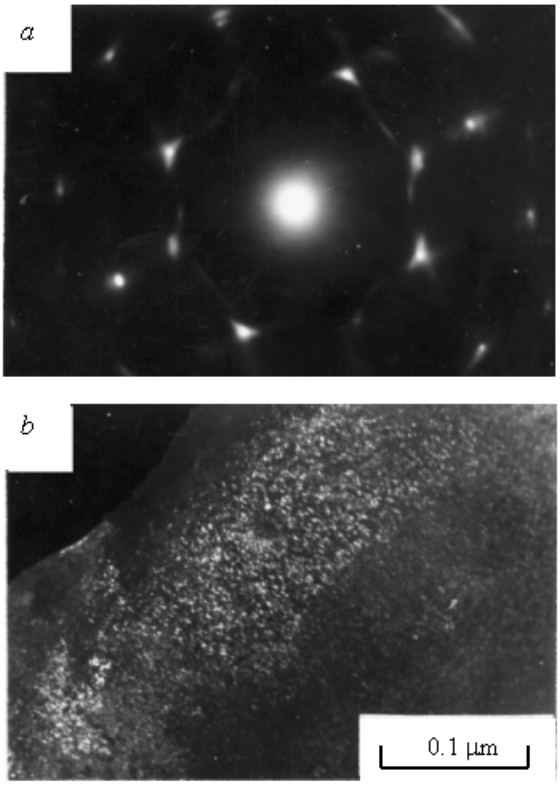

Fig. 1. Diffuse peaks of electron diffraction from Mo_2C carbide particles (*a*) and a dark-field image of these particles (*b*) in the ion-doped layer of molybdenum after II in mode I.2

Thus, under the conditions of low-temperature ($T \le 400$ K) implantation of carbon and nitrogen ions into molybdenum, highly dispersed Mo_2C and Mo_2N are formed, respectively. Estimates obtained from the data on the diffusion mobility of carbon and nitrogen atoms at $T = 400$ K [14] yield $\sqrt{Dt} \le 2$ nm, which is too small for the formation of Mo_2C and Mo_2N particles of size 3–4 nm observed in experiment. It seems that this becomes possible as a result of radiation-enhanced diffusion.

3.2. Phase composition and defect microstructure of the surface layer on radiation with doses $\ge 5 \cdot 10^{16}$ cm^{-2}

As the dose of carbon and nitrogen implant ions is increased to $5 \cdot 10^{16}$ cm^{-2}, the volume fraction of carbides and nitrides increases. A similar increase in volume fraction of the Mo_2N particles is detected on increasing the dose of nitrogen implant ions. The diffraction pattern testifies to the fact that the relative orientation of the Mo_2N and matrix fcc lattices obeys the Bain relationship [11, 15] for the irradiated Mo surface parallel to the crystallographic planes {100} and the Kurdyumov–Sachs relationship [15] for the Mo sample surface parallel to the planes {111}. The orientation relationships for the Mo_2N particles and the molybdenum matrix correspond to the minimum differences in their interplanar distances in the plane of the target and to the maximum differences in the direction normal to this plane [15].

Substantial changes in the phase-structure state are detected as the dose metal ions implanted in modes I.1 and II.1 is increased. For this case, electron diffraction patterns show extra structural peaks (Fig. 2,*a*). Analysis of the electron diffraction patterns obtained (Fig. 2,*b*) has shown that the second phase particles are carbide (Mo_2C) particles with lattice constants $a = 0.297 \pm 0.002$ nm, $c = 0.985 \pm 0.002$ nm, $c/a \approx 1.633$ and with the orientation relationship with a matrix $(10.\bar{1})$, $(\bar{1}2.0)$ $Mo_2C \parallel (100)$ Mo. An increase in temperature during II increases the carbide particle size, measured on dark-field images, from $d = 3$–7 to 10–15 nm.

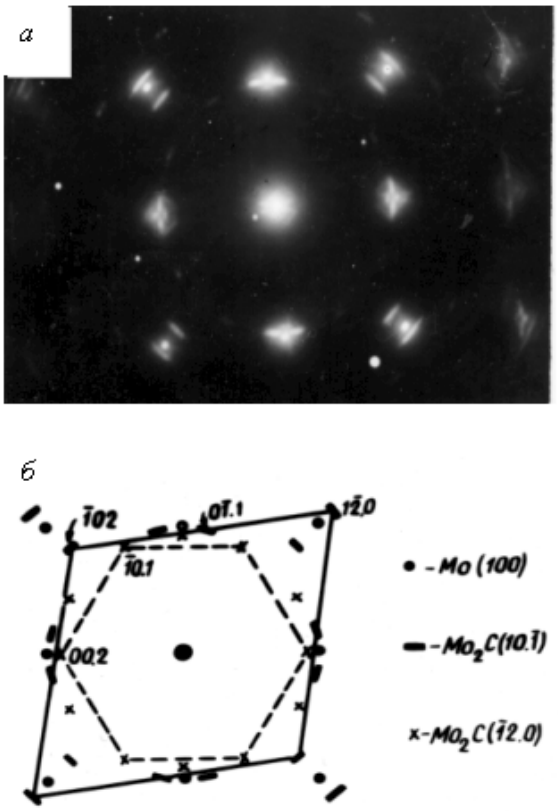

Fig. 2. Pattern of the diffraction from Mo_2C particles (*a*) and its interpretation (*b*) after self-implantation of molybdenum in mode I.1

Thus, upon high-dose implantation in a vacuum of $(1–2) \cdot 10^{-4}$ Torr, produced by diffusion pumping, the ion-modified layer a molybdenum sample is saturated with carbon as a result of surface adsorption of hydrocarbons and their ion mixing in the surface layer. Examination of the composition of this layer by the method of secondary ion mass spectrometry has shown that the thickness of the layer enriched with carbon (mode I.1) is not over 20–30 nm [12]. At elevated temperatures (modes II.1, III.2, and III.3), a contribution of radiation-enhanced diffusion to the saturation of this layer with the elements of the implanter vacuum medium (10^{-4}–10^{-5} Torr) is not improbable.

Table 2. The standard heat (–ΔH) and free energy (–ΔF) of formation of nitrides, oxides, and carbides [14, 18, 20] of the elements of the ion-doped layer

Oxides	–ΔH, kkal/mol	Carbides	–ΔF, kkal/mol	Nitrides	–ΔF, kkal/mol
Fe_3O_4	268	TiC	44.6	TiN	80.2
TiO_2	226	ZrC	44.1	ZrN	87.0
ZrO_2	264	Cr_2C_6	16.4	Cr_2N	52.0
Cr_2O_3	273	Cr_7C_3	41.7	CrN	64.0
Y_2O_3	427	Mo_2C	11.7	Mo_2N	34.4
MoO_2	141	Fe_3C	–6.4	Fe_4N	2.6

An increase in nitrogen partial pressure in this medium to $(2–4)\cdot10^{-4}$ Torr (modes III.1–III.3) is responsible for the change of the nature of the phase formed upon II. In this case, Mo_2N particles with an fcc lattice and $a = 0.418 \pm 0.002$ nm are detected by electron microscopy. The features of the formation of this phase (its orientation relative to the molybdenum matrix and dispersivity) are similar to those considered above for the case of implantation of nitrogen ions.

Second phases based of implant elements (Y, Zr, Ti) are not detected in the ion-doped layer though the enthalpy of their formation is much greater than that of molybdenum carbides and nitrides (Table 2).

Despite the low solubility of Y and Zr in molybdenum, after II at $T \le 670$ K, strongly supersaturated solid solutions of these elements in Mo [14] are observed. This seems to be due to the low diffusion mobility of Y and Zr atoms in Mo at 670 K that is evidenced by the precipitation of ZrO_2 and Y_2O_3 particles in ion-doped layers of metal foils prepared for electron-microscopic examinations which are subjected (after II) to annealing at 1273 K [13]. Formation of oxides occurs as a result of internal oxidation due to oxygenation of the surface layer at thermal treatment in a vacuum $2\cdot10^{-5}$ Torr [16].

Substantially different results have been obtained for the implantation of silicon ions into molybdenum. It turned out that at radiation doses of $\le 5\cdot10^{16}$ cm^{-2} different phase-structure states are formed in the ion-doped layer at different distances from the surface [17]. In this case, immediately near the surface, a thin amorphous film is observed, and the electron diffraction patterns show two weak diffuse halo in the absence of diffraction peaks from crystalline phases. Analysis has shown [17] that the amorphous phase is silicon-stabilized molybdenum monocarbide (MoC_xSi_y). As the dose is increased to 10^{17} cm^{-2}, particles of molybdenum silicide (Mo_3Si) and its amorphous phase are also detected [17]. Thus, when Si ions are implanted into molybdenum, different phases render amorphous at different distances from the irradiated surface, and this seems to be related to the saturation of the surface layer with carbon.

With increasing nitrogen partial pressure (mode III.1) at ion doses up to $2\cdot10^{17}$ cm^{-2}, amorphization is not detected. In this case, a single-phase film of thickness 30–50 nm having fcc structure with $a = 0.418 \pm 0.002$ nm, which coincides the lattice parameter of molybdenum nitride (Mo_2N) is observed in the surface layer. As the ion-doped layer grows in depth, a heterophase structure is detected whose electron diffraction pattern is interpreted in Fig. 3. It turned out that this heterogeneous structure is a mixture of phases: $Mo + Mo_2N + Mo_3Si + MoSi_2$, and crystal lattices of all detected phases have particular orientations relative to the lattice of molybdenum.

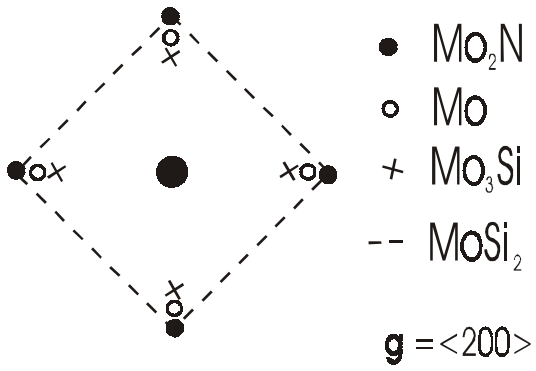

Fig. 3. Interpretation of the electron diffraction pattern from the heterophase structure of the subsurface layer for silicon-implanted molybdenum

Different phase-structure states are also observed for the implantation of high doses of carbon and nitrogen ions into Mo (mode I.2); namely, for carbon ions implanted with a dose of 10^{17} cm^{-2}, amorphization is detected with a characteristic pair of diffuse rings and diffraction peaks from the Mo_2C phase and from the molybdenum matrix of a deeper located sublayer (Fig. 4,*a*). At doses of $10^{17}–5\cdot10^{17}$ cm^{-2} there occurs complete amorphization of the ion-doped layer (Fig. 4,*b*). In this case, the amorphous phase seems to have a composition close to Mo_2C. Note, by the way, that the peak values of the carbon or nitrogen concentration obtained by the Monte Carlo calculation of their profiles at a dose of $5\cdot10^{17}$ cm^{-2} reach 30–32 at. % [12]. Nevertheless, amorphization it is not observed in the ion-doped layer at these doses of nitrogen ions: in electron diffraction patterns, the reflections from the phase Mo_2N in thin sections of the metal foil are in some cases more intense than the reflections from the molybdenum matrix. In this case, a solid Mo_2N layer is detected on the edges of the metal foil with the particle (grain) size of this phase ranging from a few to some tens of nanometers.

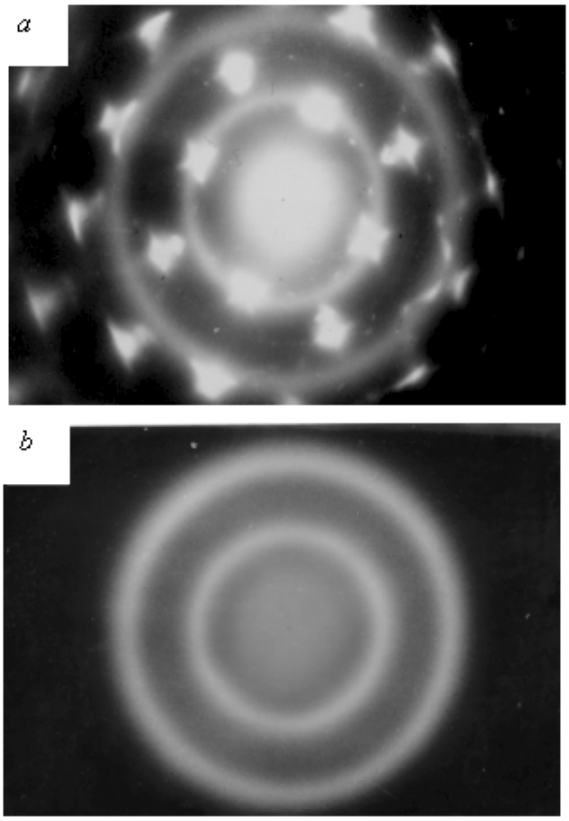

Fig. 4. Patterns of the electron diffraction in the ion-doped layer of molybdenum at high (10^{17}–$5\cdot10^{17}$ cm^{-2}) doses for the implantation of carbon in mode I.2

3.3. Phase-structure state of α-Fe and steel after high-dose ion implantation

A characteristic feature of the phase-structure states resulting from high-dose ($\geq 5\cdot10^{16}$ cm^{-2}) ion implantation in a vacuum of 10^{-4}–10^{-5} Torr in iron-base alloys is the formation of oxide phases in the ion-doped layer. In this case, while the implantation of metal ions, in particular Ti (mode IV) into α-Fe results in the formation of iron oxide (FeO) particles of size 10–12 nm, in austenitic stainless steels (mode V), type Fe_3O_4 oxides of varied dispersivity are formed. For the implantation in mode V, chaotically oriented Fe_3O_4 particles of size 5–10 nm are formed along with particles with the lattice orientation similar to that of the matrix (γ-austenite), which is testified by the coincidence of the texture maxima of the phase formed with the reflections of the matrix. As the temperature is decreased to $T = 300$ K with additional heat removal from the target, the electron diffraction patterns becomes qualitatively different in character: they show diffuse and fine continuous rings (Fig. 5,*a*). Measurement of the parameters of the diffuse rings has shown that the first (most smeared) ring can be interpreted as the result of overlap of strongly smeared diffraction peaks of type {220} and {311}, whereas the second and third ones as the diffraction reflections from the planes {400} and {440} of oxide Fe_3O_4. Estimates obtained with the use of the diffraction peak {400} have shown that the experimentally detected width of this line corresponds to a crystal size $d \leq 1$–2 nm. Since with these d values the volume fraction of the intercrystalline amorphouslike phase is comparable to that of the crystalline component, this structural state is identified as amorphous-crystalline. Presence of fine continuous rings (Fig. 5,*a*) testifies also to presence of nanocrystalline particles of a second phase having a size of some tens of nanometers.

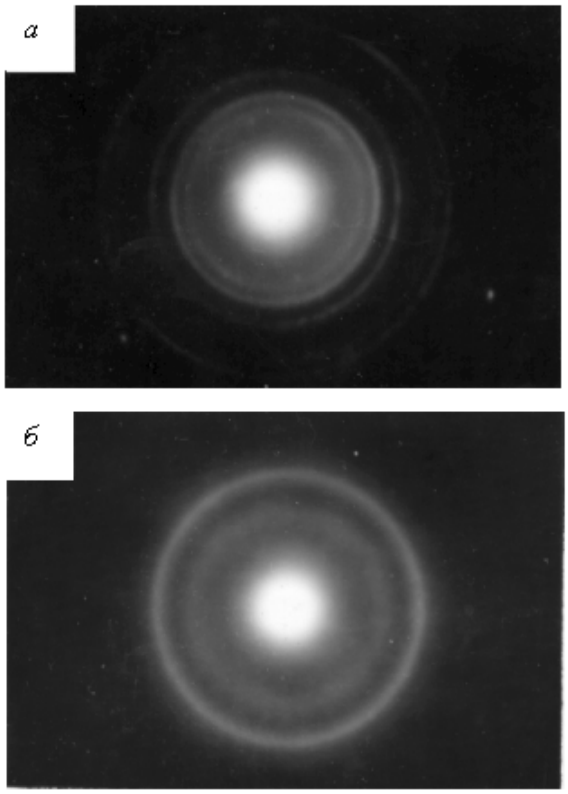

Fig. 5. Patterns of the diffraction in the ion-doped layer of steel 02X17H14M2 after II in mode V. Irradiation dose: $5\cdot10^{16}$ cm^{-2} (*a*) and $2\cdot10^{17}$ cm^{-2} (*b*).

The increase in irradiation dose to $2\cdot10^{17}$ cm^{-2} results in complete amorphization of oxides (Fig. 5,*b*). Thus, irrespective of the type of metal ions (Y, Ti, Mo, Ni, Cr), under the conditions of a vacuum of 10^{-4}–10^{-5} Torr produced by diffusion pumping, the key factor in the phase-structure modification of the surface layer of iron and austenitic stainless steels is the interaction the surface with the oxygen of the residual gas of the implanter which is accompanied by the formation of dispersed ferric oxides.

3.4. Features of the microstructure and phase composition of the surface layers of molybdenum and austenitic stainless steel after ion implantation in a cryogenic vacuum of 10^{-5}–$4\cdot10^{-7}$ Torr

Investigations have shown that in the case of cryogenic vacuum the phase-structure state of the ion-doped layer of molybdenum is governed by the inter-

action of the surface with oxygen. Depending on the degree of evacuation, molybdenum oxides of varied stoichiometry are observed to form. At a dose of Ti ions of 10^{17} cm^{-2} implanted in a vacuum of 10^{-5} Torr (mode VI.1) an amorphous phase is detected which is crystallized on heating in the electron microscope column with the formation of nanocrystalline molybdenum oxide (Mo_4O_{11}) (Fig. 6). With the degree of vacuum increased to $2\cdot10^{-6}$ Torr, the electron diffraction patterns show weak reflections of molybdenum oxide (Mo_2O_3), testifying to a considerable (no less than by an order of magnitude) decrease in volume fraction of oxide phases. In this case, a high (about $5\cdot10^{10}$ cm^{-2}) density of uniformly distributed dislocations is observed in the surface layer [19]. Under the conditions of implantation of metal ions (e.g., Y and Ti ions in a vacuum of $4\cdot10^{-7}$ Torr, see mode VI.2), second phases are not revealed immediately after implantation. However, upon subsequent annealing, particles of oxides (Y_2O_3 or TiO_2) are detected. Hence, the ion-doped layer after II is a supersaturated solid solution with the oxygen and implant element concentrations insufficient for the formation of second phases under the conditions of low diffusion mobility of these elements.

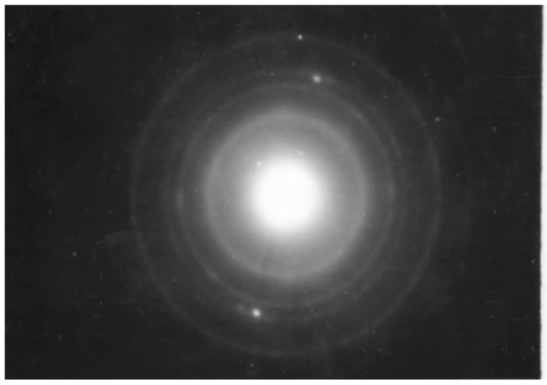

Fig. 6. Pattern of the diffraction from the surface nanocrystalline molybdenum oxide layer after II in mode VI.1

For the samples of austenitic stainless steel, the phase formed upon implantation of metal ions (mode VI.3) remains unchanged in nature. As a rule, oxides (Fe_3O_4 or Fe_2O_3) are detected. In common with molybdenum, as the degree of vacuum is increased to $2\cdot10^{-6}$ Torr, the volume fraction of these oxides abruptly drops, and at a vacuum of $4\cdot10^{-7}$ Torr second phases are not detected. In the ion-doped layer, a homogeneous dislocation pattern with a dislocation density of ~10^{10} cm^{-2} is observed. Oxides (Y_2O_3 and TiO_2) are detected after annealing of the doped samples.

4. Discussion

The results described above indicate that, irrespective of the type of metal implant ions, for the pressure range 10^{-4}–10^{-7} Torr, the degree of vacuum and the temperature in the course of ion implantation are the key factors in the modification of the phase-structure state of the surface ($\Delta h \leq 200$ nm) layer of alloys based on molybdenum and iron (including austenitic stainless steels). In this case, in a vacuum of 10^{-4}–$2\cdot10^{-4}$ Torr produced by diffusion pumping, because of the high partial pressure of hydrocarbons, carbides (Mo_2C) are formed in a molybdenum target. With the nitrogen partial pressure increased to $4\cdot10^{-4}$ Torr, nitrides (Mo_2N) are formed, whereas under the conditions of cryogenic vacuum of 10^{-5}–10^{-6} Torr, type MoO_2 oxides are observed. Hence, in this case, the partial pressure of the active gas components (C, N, O) of the residual gas of the implanter is the determining factor in the formation of second phases.

At the same time, in α-Fe and the test steel subjected to II under the same conditions, only iron oxides, predominantly Fe_3O_4, are detected. It should be noted that at doses of Y, Ti, Zr, and Cr ions up to 10^{17} cm^{-2}, compounds of these elements with oxygen, nitrogen, and carbon are not revealed, whereas upon subsequent annealing of the doped samples at $T = 1200$ K, oxides (Y_2O_3, ZrO_2, and TiO_2) are detected. Thus, immediately after implantation of Y, Zr, and Ti ions, these elements are in a solid solution.

The results obtained suggest that the structure-phase state of an ion-doped layer depends on both the II conditions and the intensity of the chemical interaction of the elements constituting the metal target with the residual gases of the implanter adsorbed on the target surface.

First of all, the possibility of the formation of second phases in an ion-doped layer is determined by the level of diffusion mobility of atoms. In view of this, we used the data reported elsewhere [19, 20, 21] to estimate the diffusion constants D for interstitial and substitutional impurity atoms in the test α-Fe, Mo, and steel at $T = 500$ K. It turned out that for C, N, and O atoms, values of D lie in the range 10^{-9}–10^{-11} cm^2/s in α-Fe and in the range 10^{-13}–10^{-19} cm^2/s in Mo. For substitutional atoms, D values are close to ~10^{-40} cm^2/s in Mo and ~10–30 cm^2/s in steel. Thus, the diffusion ranges of interstitial atoms in α-Fe and Mo appear to be, respectively, $\Delta X_1 \approx 10^{-4}$ cm and $\Delta X_2 \approx 10^{-5}$–$10^{-7}$ cm. For substitutional atoms, we have $\Delta X_1 \approx 10^{-13}$ cm for steel and $\Delta X_2 \approx 10^{-18}$ cm for Mo. Hence, even under the conditions of radiation-enhanced diffusion, the diffusion paths of substitutional atoms do not reach values of 1–10 nm, which are necessary for the formation of second phase particles based on implant elements, whose concentration, even at a dose of 10^{17} cm^{-2}, is not over 5–10 at. %.

At the same time, the formation of carbides, nitrides, and oxides with atoms of the target material appears possible because it does not call for diffusion flows of these atoms. It is also not improbable that the redistribution necessary of atoms necessary for the formation of compounds Mo_2C, Mo_2N, and Fe_3O_4 is promoted by the local heat release associated with the formation of a chemical compound.

The reasons presented above are well confirmed by the data on the heat and free energy of formation of nitrides, oxides, and carbides with elements of the ion-doped layer of test targets [14, 18, 20] (Table 2). As can be seen from Table 2, Y, Zr Ti, and Cr have the maximum heat or free energy of formation of compounds with active elements of the gas medium of the implanter (N, C, O). In this case, from the point of view of chemical interaction, the formation of oxides is most probable. However, we have detected the latter only in α-Fe and in stainless steel, while oxides of implant metals, such as Y_2O_3, ZrO_2, and TiO2 are detected only after annealing at 1200 K. It seems that the factor of chemical affinity, being slightly different for MoO_2, Mo_2C, and Mo_2N, appears not as substantial as the influence of the partial pressure of hydrocarbons for the vacuum $(1–2)\cdot10^{-4}$ Torr produced by diffusion pumping or for bleed-in of nitrogen to a pressure of $4\cdot10^{-4}$ Torr (see Table 1). This is well evidenced by the formation of MoO_2 (instead of Mo_2C and Mo_2N) in a cryogenic vacuum of 10^{-4}–10^{-6} Torr.

Thus, by properly choosing the conditions of II, in particular, by varying the degree of vacuum in the implanter, it is possible to vary the nature and volume fraction of second phases in the ion-doped layer and, accordingly, the strength, tribological, and corrosion characteristics of materials and articles treated by the II method.

The low diffusion mobility of atoms during II is responsible not only for the nature of the phase formed, but also for its dispersivity. Since in this case the processes of coagulation of second phases are practically suppressed at an increased irradiation dose (and time), the particle size is not over 4–5 nm. With increasing the temperature of implantation (modes II–I, III.3, Table 1), the particle size increases to some extent ($d \le 15$ nm). Nevertheless, at a high volume content of second phases, either nanophase or amorphous-crystalline phase ($d < 2$ nm) is formed in the surface layer.

Under the conditions of cryogenic vacuum of $4\cdot10^{-7}$ Torr, second phases are not detected, and the lattice curvature substantially decreases, though the dislocation density in the surface layer reaches $(2–5)\cdot10^{10}$ cm^{-2}. In the case of II of yttrium with a dose of 10^{17} cm^{-2}, an anomalously supersaturated Mo–Y solid solution is formed [19]. Nevertheless, amorphization of the ion-doped layer is not observed.

This work has been supported in part by the Ministry of Education of the Russian Federation and by CRDF within the framework of the BRHE (project TO 016-02).

References

[1] F.F. Komarov, *Ion Implantation into Metals* (in Russian), Moscow, Metallurgia, 1990.

[2] A.N. Tyumentsev, A.D. Korotaev, Yu.P. Pinzhin et al., Fiz. Met. Metalloved, No. 9, 131 (1992).

[3] A.N. Tyumentsev, A.D. Korotaev, S.P. Bugaev, Russian Phys. Journ. **37**, No. 5, 452 (1994).

[4] A.D. Korotaev, A.N. Tjumentsev, Izv. Vyssh. Uchebn. Zaved. **37**, No. 8, 3 (1994).

[5] A.N. Tyumentsev, A.D. Korotaev, Yu.P. Pinzhin et al., Fiz. Met. Metalloved. **83**, No. 5, 80 (1997).

[6] D.M. Follstadt, J. Appl. Phys. **51**, No. 2, 1001 (1980).

[7] D.M. Follstadt, J.A. Knapp, L.E. Pope, F.G. Yost, S.T. Picraux, Appl. Phys. Lett. **45**, No. 5, 529 (1984).

[8] Yu.A. Bykovskii, V.S. Kulikadekas, A.M. Markeev, V.I. Nevolin, and V.Yu. Fominskii, Poverkhnost, No. 4, 129 (1986).

[9] M. Iwaki, K. Yobe, M. Suzuki, O.N. Ihimura, Nucl. Instr. Meth. in Phys. Res. **B19/20**, 150 (1987).

[10] S.P. Bugaev, E.M. Oks, P.M. Schanin, and G.Yu. Yushkov, Prib. Tekh. Exper, No. 6, 125 (1990).

[11] A.N. Tyumentsev, A.D. Korotaev, Yu.P. Pinzhin, Yu. R. Kolobov, S.P. Bugaev, P.M. Schanin, G.Yu. Yushkov, Nucl. Instr. & Methods in Phys. Res. **B 80/81**, 491 (1993).

[12] A.D. Korotaev, A.E. Behert, A.N. Tyumentsev, and S.P. Bugaev, Russian Phys. J. **37**, No. 2, 109 (1994).

[13] A.N. Tyumentsev, A.D. Korotaev, Yu.P. Pinzhin, A.F. Safarov, S.P. Bugaev, A.G. Nikolaev, and G.Yu. Yushkov, Fiz. Met. Metalloved. **83**, No. 2, 110 (1997).

[14] E. Fromm, E. Gebhardt, *Gaes and Carbon in Metals*, Moscow, Metallurgia, 1980, 712 pp.

[15] A.N. Tyumentsev, A.D. Korotaev, Yu.P. Pinzhin et al., Fiz. Met. Metalloved., No. 9, 123 (1992).

[16] A.D. Korotaev, A.N. Tyumentsev, and V.F. Sukhovarov, *Dispersion Hardening of Refractory Metals* (in Russian), Moscow, Nauka, 1989.

[17] A.N. Tyumentsev, A.D. Korotaev, Yu.P. Pinzhin, A.F. Safarov et al., Physics of metals and metallography **83**, No. 5, 516 (1997).

[18] *High-Melting Compounds* (in Russian, ed. by G.M. Samsonov and I.M. Vinitskii), Moscow, Metallurgia, 1976.

[19] A.N. Tyumentsev, S.V. Ovchinnikov, A.D. Korotaev, Yu.P. Pinzhin, M.V. Lupachyov, A.G. Nikolaev, G.Yu. Yushkov, Fiz. Met. Metalloved. **93**, No. 5, 60 (2002).

[20] *Phase and Chemical Properties of Oxides* (in Russian, ed. by G. M. Samsonov), Moscow, Metallurgia, 1978.

[21] *Structure and Properties of Metals and Alloys* (in Russian, ed. by L.N. Larikova and V.I. Isaicheva), Kiev, Naukova Dumka, 1987.